

# Direct metallisation of polyetherimide substrates by activation with different metals

*Dr Thomas D.A. Jones\*<sup>1,3</sup>, Assel Ryspayeva<sup>1</sup>, Dr Mohammadreza N. Esfahani<sup>2</sup>, Matthew P. Shuttleworth<sup>2</sup>, Professor Russell A. Harris<sup>2</sup>, Dr Robert W. Kay<sup>2</sup>, Professor Marc P.Y. Desmulliez<sup>1</sup> and Dr Jose Marques-Hueso<sup>1</sup>*

<sup>1</sup>*Heriot-Watt University, School of Engineering & Physical Sciences, Nature Inspired Manufacturing Centre, Edinburgh EH14 4AS, Scotland, UK*

<sup>2</sup>*Future Manufacturing Processes Research Group, School of Mechanical Engineering, University of Leeds LS2 9JT, England, UK*

<sup>3</sup>*University of Dundee, School of Science & Engineering, Dundee DD1 4HN, Scotland, UK*

## Abstract

This article reports the performance of different metallic ions and nanoparticles (Ag, Cu, Ni, Pd, Cr, Co, Au and Fe) used as seed layers, formed by chemical or optical reduction, for the electroless Cu plating of metal tracks onto polyetherimide (PEI). Plated Cu performance was tested by adhesion, electrical conductivity, plating rate, XPS, SEM, XRD and EDX analysis. The application of Cu and Ag seeds resulted in high quality electroless Cu deposits presenting strong adhesion properties and high conductivity ( $(2.0 \pm 0.5) \times 10^7$  S/m and  $(3.6 \pm 0.2) \times 10^7$  S/m, respectively) compared with bulk copper ( $5.96 \times 10^7$  S/m). Performance is attributed to the high surface density and uniformity of seed layers. Of the metals, only Ag ions were photoreduced under the conditions applied and were subsequently used to electroless Cu plate high quality track features of 150  $\mu\text{m}$  width. The application of sulphuric acid pre-treatment to PEI prior to Ag ion exchange, improved the photoinitiated track formation process, as demonstrated by a threefold increase to both photoinduced Ag nanoparticle density on the surface and electroless Cu plating rate, as well as improved electroless Cu adhesion to PEI.

## Key Words

Direct Metallisation; Photoreduction; Polyetherimide; Electroless Copper; Metal Catalyst; Electrical Interconnect.

## 1 Introduction

High temperature plastics are ubiquitous in aerospace, space, solar industry, consumer electronics, automotive, defence and medical applications. The compound annual growth rate of high temperature plastic materials is projected to be at 7.5 % between 2016 and 2024,

reaching a market value of \$1.77 Bn, with the growth being driven by thin photovoltaics, wearable electronics and sensing [1]. Polyetherimide (PEI) is a high temperature plastic ( $T_g=217^\circ\text{C}$ ) offering thermal stability, mechanical strength, high radiation and chemical resistance, good adhesion, and a low dielectric constant [2,3]. For these reasons this material is suited to high value, high temperature applications, but has additional applications in additive manufacturing[4]. The polymer can be 3D printed by FDM (fused deposition modelling) or casted by injection moulding. Work by the authors highlighted the possibility of direct metallisation of PEI surfaces [3], and selective direct metallisation (DM) of electrical micro-circuitry onto PEI, using a silver (Ag) catalyst and visible light, followed by electroless copper (Cu) plating [5]. This process was enhanced on the application of a wet photocatalyst sensitizer potassium chloride (KCl), which decreased the photoreduction time from several hours to seconds[6]. The application of KCl to an ion exchanged Ag-PEI substrate causes the formation of photosensitive compound AgCl, which can then be photoreduced to silver (Ag) metal by visible light (450 nm), as confirmed by EDX and XRD, respectively, in previous work[5]. The selective production of metallic nanoparticles via  $m^+$  reduction can be achieved by either using light, heat[7,8], chemistry[9], or by high energy radiation[10,11]. Chemical reduction is popular due to its relative simplicity and low cost[9]. Selective plating can be obtained using a local chemical reduction method[12], whereas optical reduction allows for selective activation and direct metallisation of the surface, without the use of costly additional processing[13].

In this work, investigations of chemical and optical reduction onto PEI are carried out using the transition metals: palladium (Pd), gold (Au), Ag, copper (Cu), nickel (Ni), iron (Fe), cobalt (Co) and chromium (Cr). The transition metals act as catalysts for electroless Cu plating and so, activate PEI for electrical track formation [12]. Transition metals are applied due to their ability to change oxidation state or absorb other substances onto their surface [14]. The activation of a surface and the quality and success of subsequent metal deposition varies depending on the metal catalyst used [15]. Their concentration, temperature and processing time also influence the fabrication of high-quality circuitry by electroless plating [16]. The catalyst Pd has the highest catalytic activity and additionally shows the highest stability, which enables it to remain in its metallic state for longer to act as a catalyst [17,18]. Au and Ag both display a high catalytic activity and low susceptibility to oxidation [19]. These three metals are all costly due to their rare earth metal status, but cheaper alternatives are possible with Cu, Ni and Fe, that have been successfully demonstrated for electroless plating [12,20,21]. Co nanoparticles display a high functionality and are used in many advanced chemical and physical applications [22], and so, incorporating Co nanoparticles into PEI surfaces is of

interest. Cr has uses as a refractory layer and is economic, and so its application to PEI flex is also of interest [23,24]. For the different metal catalysts, it is highly desirable to identify what processing conditions enable effective electrical circuitry formation on PEI.

The metals also display different degrees of biocompatibility[25,26], costs per unit weight, ability to act as diffusion barriers[27], and potential for creating magnetic alloys[28]. Fabricating circuitry using the different metals has applications in high value manufacture of bio-medical devices[29], sensors[30–32] or data storage units, warranting investigations into the embedding of these metals into PEI. It is desirable to form selective circuitry optically using the different metals as catalytic seed and so, their ability to be reduced onto PEI is tested first by using chemical reduction. The quality of the chemically and optically reduced metal catalysts is evaluated from observations of nanoparticle (NP) morphology and density, as these parameters influence their chemical activity[33]. The ability of the different metals to act as catalytic layers to receive high quality Cu deposits, is therefore reviewed in terms of Cu adhesion and conductivity. A strong adhesion of Cu to PEI and a fast processing time are desirable for long circuit lifetime and low manufacturing costs, respectively [34,35].

A strong adhesion of Cu to PEI and a fast processing time are desirable for long circuit lifetime and low manufacturing costs, respectively [34,35]. The photoreduction rate is enhanced on the application of the KCl photosensitizer, with rates increasing with sensitizer concentration up to a limiting value defined by mass transfer [36]. Studies are thus performed here to further improve processing rates by increasing the pre-processing and to identify the minimum KCl concentration which provides both a fast photoreduction time, and a high nanoparticle surface density.

## **2 Experimental Procedure**

The metallisation process was performed as outlined in Figure 1.

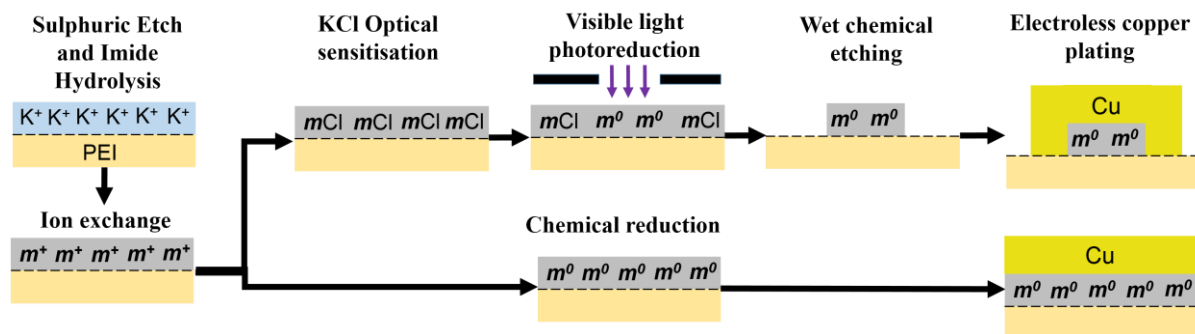


Figure 1 – Process flow for the incorporation of metal catalyst onto PEI by optical and chemical reduction. The resulting conductive layer acts as a seed for electroless plating. Not to scale.

The PEI surface is first hydrolysed, breaking imide bonds to form amide bonds, which can then receive potassium ions, that are ion exchanged with the desired metal cation ( $m^+$ )[3]. Light of wavelength in the visible spectrum, selectively exposes and induces the photoreduction of the  $m^+$  ions into metallic nanoparticles ( $m^0$ ). In the regions unexposed, metal ions remain on the surface. These ions are unwanted and so a wet chemical etch is applied that selectively removes the unexposed metal ions, leaving reduced metal nanoparticles. The nanoparticles remaining on the surface after etching provide active sites for electroless plating.

PEI 75  $\mu\text{m}$  thick flexible sheets grade 1000B ULTEM was supplied from Cadillac, Plastics, UK. The remaining chemicals were supplied by Fisher Scientific, UK. The processing conditions for the different experiments are outlined in Table 1.

Table 1 – Processing conditions for PEI

Processing stage	Processing condition	
1. Substrate clean	40 kHz Ultrasound DI rinse (Ultrawave IND5040D) for 20 min, isopropanol de-grease.	
2. Pre-treatment	18 M $\text{H}_2\text{SO}_4$ Acid dip for 3 min at 25°C, DI water rinse for 4 min, 15 M KOH dip for 20 min at 50°C, DI water rinse for 4 min.	
3. Metal ion-exchange	Copper: 0.1 M $\text{CuSO}_4 \cdot 5\text{H}_2\text{O}$ , 60 min at 50°C Nickel: 0.2 M $\text{NiSO}_4$ , 60 min at 50°C Palladium: 0.1 M $\text{PdCl}_2$ , 20 min at 20°C Gold: 0.03 M $\text{HAuCl}_4 \cdot 3\text{H}_2\text{O}$ , 150 min at 20°C Silver: 0.1 M $\text{AgNO}_3$ , 20 min at 20°C Iron: 0.1 M $\text{FeSO}_4$ , 60 min at 20°C Cobalt: 0.1 M $\text{Co}_3\text{O}_4$ , 5 min at 50°C Chromium: 0.1 M $\text{CrCl}_3 \cdot 6\text{H}_2\text{O}$ , 60 min at 50°C DI water rinse after all metal treatments.	
4. Reduction method	<b>Chemical Reduction</b> 1.0 M $\text{NaBH}_4$ , 60 min at 50°C, with stirring.	<b>Optical Reduction</b>

		Sample immersion in 0.01 M KCl (ethanol:water, 3:1) for 60 seconds, followed by irradiance through a Chromium mask by a 460 nm, (1 W) LED for 60 seconds.
<b>5. Selective etch</b>		15 seconds in 17 % ammonia (17%) followed by 20 seconds in 5 % sulfuric acid and with DI water rinse after all treatments.
<b>6. Electroless copper plating</b>		Plated in an electroless copper solution comprising 15 g/L copper (II) sulphate pentahydrate, 70 g/L sodium potassium tartrate, 20 g/L sodium hydroxide, and 77 mL/L formaldehyde 37%, for a period between 20 and 30 min at 20 °C.

Different metal catalyst solutions were chosen for ion exchange with PEI based on their exchange success with  $K^+$  ions embedded into PI. The concentration for each solution is outlined in Table 1 and the values were chosen from literature sources. The literature sources includes Gold (III) chloride trihydrate[37], Palladium (II) chloride[16], Cobalt (II,III) oxide[22], Copper sulphate pentahydrate[12], Nickel (II) sulphate hexahydrate[20], Iron (II) sulphate[21] and Silver nitrate[5]. An additional metal considered for reduction is Chromium (III) chloride, due to its low cost. The durations and temperatures chosen for metal catalyst immersion differ and were based on the catalytic activity of the metals. Pd displayed the highest activity of the metals and so has a short ion exchange immersion duration, which was performed at room temperature[17]. Cu and Fe have lower catalytic activities and so their ion exchange was performed at higher temperatures and for longer durations. The temperatures and durations for the remaining catalysts were chosen based on times applied in literature and on their success obtained in the work. Different metals require reducing agents of varying type and strength to successfully reduce[15]. Sodium borohydride ( $NaBH_4$ ) is a powerful chemical reducing agent suitable for neutral or acidic solutions[38] and so, for consistency, is applied to all metals used in chemical reduction in this study. The metal catalysts require different immersion durations within the reducing agent, to reduce and so for consistency, a large reduction immersion time is applied to all. All solutions in experiments were prepared under atmosphere. Selective photoreduction is performed on all metals which display successful ion exchange onto PEI. An optical chrome glass mask, supplied by JD Photo-data Ltd. was used to enable selective exposure. The optical sensitizer KCl is applied to all and exposed with a 460 nm LED at 1 W. Unless stated, the KCl is 0.01 M in a composition of 3:1, ethanol/DI water[5]. Work was performed looking at variations to photoreduction performance for different concentrations of KCl onto Ag catalyst. The KCl concentrations investigated were 0.005 M, 0.01 M, 0.05 M, 0.1 M and without KCl.

X-ray Photoelectron Spectroscopy (XPS) measurements were performed using an SPECS FlexMod hard X-ray UHV module for electron spectroscopy under settings pass-

energy 30 eV and 35  $\mu\text{m}$  flood gun at 4 eV, for a source of 400W Al k-alpha. Samples under scan were untreated PEI; ion-exchange PEI containing ions of Ag, Cu, Ni, Pd, Au, and Fe; the same surfaces after metal ion reduction by a chemical process; and Ag NP photoreduced on PEI. Fourier–transform infrared spectroscopy (FTIR) measurements were obtained with a Perkin-Elmer Spectrum 100 FT-IR spectrometer in attenuated total reflection (ATR) mode. X-ray Diffraction (XRD) measurements were performed with a D8 Discover, from Bruker Corporation ( $\lambda = 0.15418 \text{ nm}$ ). Measurement of the FWHM of the XRD peak approximates the minimum average crystalline size  $D$  of the nanoparticles using the Scherrer equation[3]:

$$D \approx \frac{K\lambda}{\beta \cos \theta} \quad (1)$$

where  $K$  is a dimensionless shape factor (0.9, standard value [3]),  $\lambda$  is the X-ray wavelength (0.154 nm),  $\beta$  is the line broadening measured at FWHM after subtracting the instrumental line broadening and  $\theta$  is the Bragg angle measured for peak.

Scanning Electron Microscope (SEM) images were taken using a Quanta 3-D FEG. Optical absorbance was measured using a Perkin-Elmer LAMBDA 950 UV–Vis Spectrophotometer, with baseline correction performed on untreated PEI. Energy dispersive X-ray (EDX) measurements were performed with an Oxford Instruments X-maxN 150 mm EDX detector. From an SEM image of size  $11.2 \mu\text{m}^2$ , NPs were identified and their areas measured using the software ImageJ, from The Nation Institute of Mental Health (NIMH, US). Every individual particle/cluster area measured was approximated to a circle and its diameter ( $d_i$ ) evaluated. The diameters were then plotted using software Origin with the histogram function. The number average particle diameter ( $D_n$ ) was evaluated for each metal catalyst.

The particle-diameter dispersity ( $\mathcal{D}$ ), historically referred to as polydispersity index[39], was evaluated for each nanoparticle as,

$$D_w = \frac{\sum d_i^4}{\sum d_i^3} \quad (2)$$

$$\mathcal{D} = \frac{D_w}{D_n} \quad (3)$$

where  $D_w$  is the weight-averaged diameter.[40]

Electroless Cu plating was performed under conditions outlined in the experimental section of [5]. Five measurements of the pH were taken before and after each plating cycle using a Hanna-Instruments<sup>TM</sup> Hi 9110 probe. After plating, the Cu thickness was evaluated using a Bruker Dektak 3 Profilometer and the average of ten thicknesses obtained in  $\mu\text{m}$  ( $x$ ), along with the arithmetic average roughness ( $Ra$ ) evaluated by the Dektak software. From the thickness, the average electroless Cu plating rate ( $v$ ), expressed in  $\mu\text{m/hr}$ , was calculated as:

$$v = x/t \quad (4)$$

where  $t$  is the plating time in hours.

10 measures of deposit electrical resistance were obtained using a two-point probe, Signatone probe station and the average converted to conductivity with average deposit thickness ( $x$ ). Tape test analysis was performed on the electroless Cu deposits to evaluate deposit adhesion to PEI. Tests were performed as outlined under[41]. Plating quality with the inclusion of  $\text{H}_2\text{SO}_4$  pre-treatment was evaluated qualitatively from high resolution images obtained with a Leica DM5000 microscope.

### 3 Results and discussion

#### 3.1 Reduction of metal catalysts

Exchange of the potassium ions embedded in the hydrolysed PEI was attempted with ions of the following metal catalysts - Ag, Cu, Ni, Pd, Co, Cr, Au and Fe. Chemical reduction was then performed on each of the treated PEI surfaces to test their ability to form NP on PEI and to act as seed layers for electroless Cu plating.

Figure 2 shows the XPS spectra for the metal ions successfully reduced onto PEI surfaces, which includes in the inserts Ag, Cu, Ni, Pd, Au and Fe. The spectra for an unprocessed PEI surface shows the peaks for C 1s at  $\sim 284.0$  eV, N 1s at  $\sim 400.0$  eV and O 1s at  $\sim 532.0$  eV which are as expected for PEI [42]. After Ag ion exchange, the Ag 3d peak  $\sim 369.2$  eV is observed which coincides with ionic silver peak for Ag(III) [43], and after chemical reduction, Ag 3d peak at  $\sim 369.0$  eV corresponding to nanoclusters of metallic silver [44]. After Cu ion exchange, a Cu 2p at  $\sim 934.0$  eV is present that shifts to  $\sim 937.0$  eV on exposure to chemical reducing agent. The two peaks correspond to oxides of Cu [45]. After Ni ion exchange, a Ni 2p at  $\sim 857.5$  eV is observed corresponding to ionic Ni from  $\text{NiCl}_2$ , the salt used for its ion exchange[46]. After exposure to chemical reducing agent, a Ni 2p at  $\sim 856.0$  eV is present which corresponds with an oxide of Ni [47]. After Pd ion exchange, Pd 3d at  $\sim 338.0$  eV and  $\sim 343.0$  eV are observed which correspond to ionic Pd from  $\text{PdCl}_2$ , the salt used for its

ion exchange [48]. After exposure to chemical reducing agent, weak peaks of Pd 3d at ~337.0 eV and ~347.0 eV are present that correspond to oxidised Pd [49]. After Au ion exchange, a peak Au 4f at ~84.4 eV is observed that corresponds to Au(I) [50] and the peaks Au 4f7 at ~84.0 eV and 4f5 ~88.0 eV after exposure to chemical reducing agent, which correspond to bulk gold values [51]. After Fe ion exchange, a peak at ~712.0 eV coincides with Fe(II) [52]. A Fe peak was not detected for the chemically reduced sample likely due to handling. The Cu, Pd, Ni and Fe samples show oxidation which is likely to have occurred due to their time under air-atmosphere after treatment and before XPS [53,54], as the samples were exposed to a strong reducing agent, NaBH<sub>4</sub> which should not have induced oxidation.

The different XPS spectra indicates the successful ion exchange of all metal ions Ag, Cu, Ni, Pd, Au and Fe onto PEI and the chemical reduction of Au and Ag. Au and Ag elements show low oxidation [19] and so, observation of their metallic states after reduction is not surprising. To observe the other elements metallic states after reduction, storage under an inert atmosphere before XPS could be applied [53].

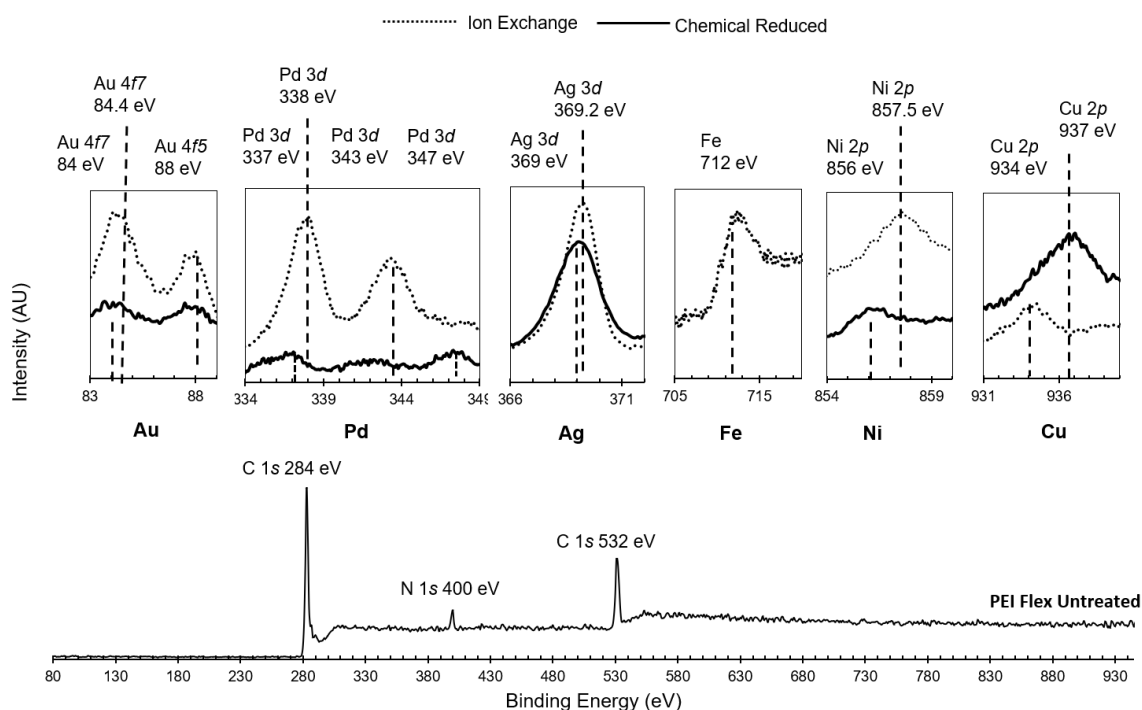


Figure 2 – XPS spectra for Unprocessed PEI, with inserts showing metal ions after ion exchange (dotted line) and chemical reduction (solid line) on PEI.

Figure 3 displays the histogram plots of the nanoparticles (NP) which were successfully reduced onto the PEI surfaces. SEM inserts of the NPs formed on the PEI surfaces are also included in each histogram. The features identified in the SEM images are nanoclusters formed



due to coalescence of smaller NPs[55]. The formation mechanism of these clusters is well reported and comprised an initial growth of the NPs, a secondary nucleation and a ripening, defined as the redistribution of mass within a nano-island or between nano-islands[56]. NP growth is initiated once chemical reduction begins, with additional secondary nucleation reactions occurring onto the particles, feeding their growth from particle to cluster. To lower surface energy, diffusion of clusters and NPs occurs forming larger structures by Ostwald ripening[57]. The ripening of the NPs eventually leads to the formation of a single deposit covering the whole substrate surface. The occupation probability of a NP describes the probability of a particle randomly existing in a location. Occupation probability values below a threshold, called the percolation threshold, describe NPs with no long range order[58]. The shape and distribution of the synthesized particles differ between metals and are influenced by their ion exchange onto hydrolysed PEI surfaces and their respective chemical reduction[15]. The concentrations and temperatures applied in these two processes can be altered to produce the desired outcome. As such, the temperature and concentration of the different metal ions solutions were selected based on successful process conditions reported in the literature[5,12,16,20–22,37]. To apply consistency between samples during the reduction process, the same reducing agent,  $\text{NaBH}_4$ , was used using identical operational conditions for all metals.

For Cu and Pd, the majority of particle diameters deposited are less than 50 nm. At this size and distribution, the NPs are well below the percolation threshold. The Au and Fe metals showed a sparser deposit, favouring the formation of clusters of size 100 nm. The particle distribution is still below the percolation threshold, but significant clustering and ripening have occurred. The Ag and Ni NPs show a high coverage of the surface with cluster sizes being more widely distributed. The Ni deposit is closest to its percolation threshold and shows evidence of particle ripening. Catalyst activity is directly related to the size of the NPs formed, whereby smaller NPs are associated with higher activity, as evidenced by the greater amount of hydrogen effluence produced in electroless Cu plating[59]. A reduction in particle size provides a larger surface area enabling faster plating rates. For this reason, the smaller NPs sizes produced with Ag, Cu and Pd help increase the plating rate of electroless Cu deposition.

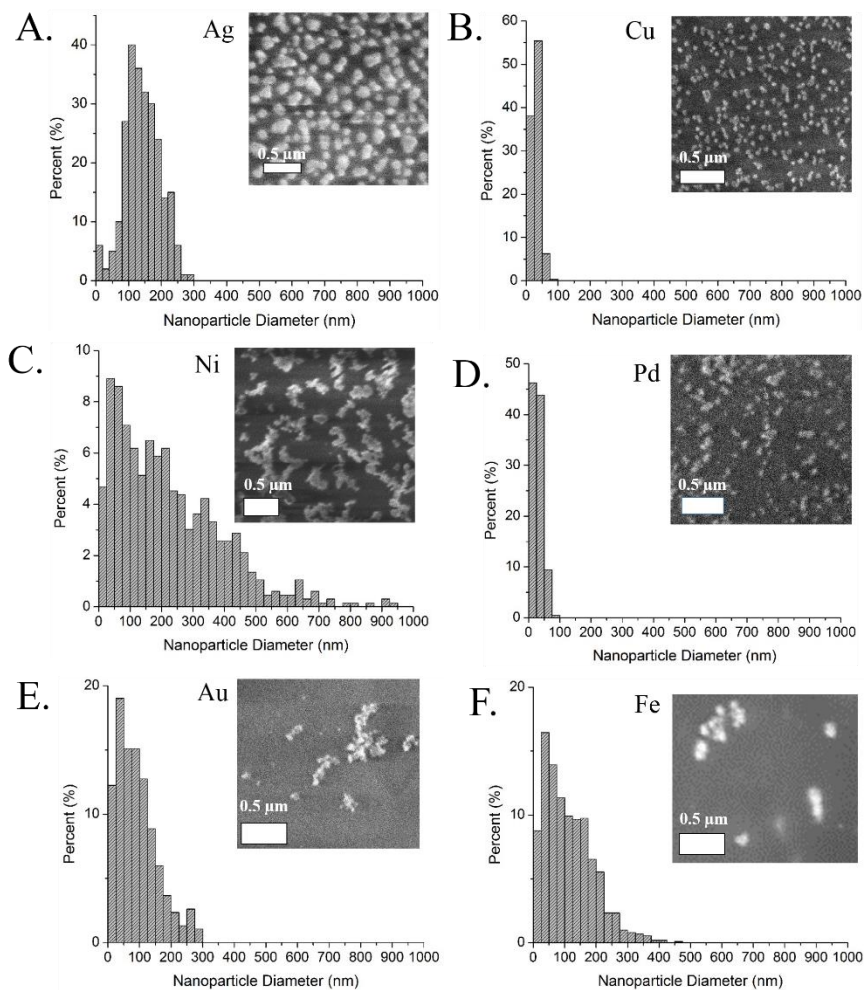


Figure 3 – Histograms of NPs size with SEM insets of NPs on PEI surface, formed after chemical reduction for A) Ag, B) Cu, C) Ni, D) Pd, E) Au and F) Fe.

The density of NPs was measured from the SEM images as shown in Table 2.

Table 2 – Summary of nanoparticle / nanocluster composition.

Metal	Optical reduction	Chemical reduction	Number averaged diameter ( $D_n$ ) $\pm \sigma$ (nm)	Dispersity ( $\bar{D}$ )	Surface particle density measured from SEM ( $\text{count}/\mu\text{m}^2$ )	EDX composition of surface
Silver	Successful[5]	Successful	$140 \pm 50$	1.4	25	Values from[5] C = 80 %, O=10%, Ag = 7%, Cl = 2%, K = 1%
Copper	Unsuccessful	Successful	$30 \pm 15$	1.6	120	C = 76%, O = 19%, Cu = 5%
Nickel	Unsuccessful	Successful	$220 \pm 170$	2.4	0.040	C = 69%, O = 22%, Ni = 5%, Na = 4%
Palladium	Unsuccessful	Successful	$30 \pm 20$	1.9	200	C = 80%, O = 18%, Pd = 2%
Gold	Unsuccessful	Successful	$90 \pm 60$	2.2	3.0	C = 79%, O = 20%, Na = 0.5%, Au = 0.5%
Iron	Unsuccessful	Successful	$110 \pm 80$	2.2	2.0	C = 74%, O = 22%, Na = 2.8%, Fe = 1.2%
Cobalt	Unsuccessful	Unsuccessful	N/A	N/A	N/A	N/A
Chromium	Unsuccessful	Unsuccessful	N/A	N/A	N/A	N/A

Pd, Cu and Ag show the highest densities of NPs and therefore the highest surface coverage, an important property for the uniformity of the electroless Cu deposited thereafter. Spaces between metallic catalysts lead to increases in inter-pore spacing within electroless deposits, which can have a detrimental effect in terms of ductility and roughness[35,55,56]. The dispersity of the NPs diameter was greater than 1 for all particles, indicating an overall low uniformity[40], although Ag and Cu showed the highest uniformity. For a high catalytic activity and coverage, a small NP size combined with high NP density and diameter uniformity is desirable. Of all the metals tested, Cu, Ag and Pd show the most preferred properties.

Optical microscopy and XRD analysis failed to show any sign of chemical reduction onto the treated PEI surfaces for the catalysts Cr and Co. Additionally, after the ion exchange or reduction processes, no Cu plating was observed when the samples were immersed in an electroless solution. In solution, Co displays a high level of agglomeration due to Van Der Waals attraction between particles, requiring usually a capping agent such as oleic acid to control particulate growth[60]. A capping agent was not applied in this study and agglomeration of Co particles in solution occurred, leading to a loose, granular deposit forming on the PEI surface. If a capping agent is applied first to the Co solution then smaller particle sizes would form and ion exchange could have been more successful; additionally thermal curing after ion exchange could have assisted reduction and adhesion[22]. Cr showed little indication of ion exchange or reduction. Ion exchange reactions with Cr (III) typically employ the use of a strong ion exchange agent[23] or physical vapour deposition[24]. In this work the hydrolysed PEI was not sufficient to exchange the Cr (III) ions.

Analysis was performed on the NP deposits to identify the elements present. Figure 4A displays the UV-Vis absorption peaks for chemically reduced metal NP onto PEI. PEI displays a high absorption below 375 nm and, as such, metallic peaks lower than this value are difficult to differentiate, which is the case for Ni, Fe and Pd. An Au peak around 540 nm was also not observed which was likely due to its low surface particle density, as indicated in Table 2. A peak on the Cu treated sample at around 610 nm coincides with the reported plasmon resonance value for Cu NPs. A peak at around 404 nm on the Fe sample indicates the presence of Fe<sub>2</sub>O<sub>3</sub>[61] due to the oxidation of Fe[53]. A peak at 435 nm was observed on the Ag sample, which coincides with its plasmon resonance value. As shown in Figure 4A, the Cu absorption over the entire scan range was greater than that of Ag or Fe as the area under the UV-Vis absorption curve is proportional to a sample's NPs concentration[62]. This observation is further corroborated by the measured larger surface particle density as indicated in Table 2.

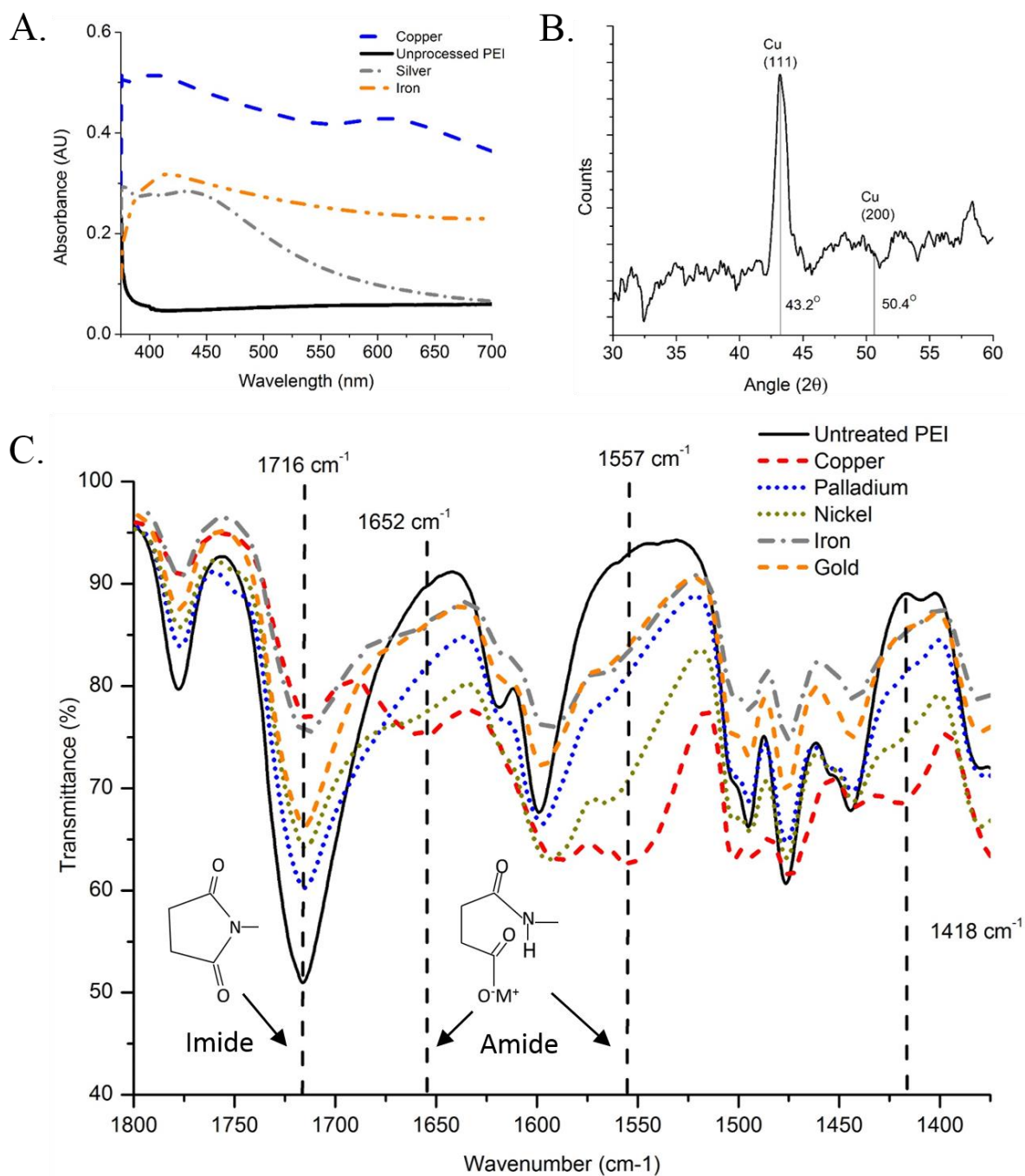


Figure 4 – Analysis of metallic NPs formed by chemical reduction, using A) UV-Vis spectroscopy, B) XRD scan of Cu and C) FTIR.

XRD scans were performed on the Cu, Ni, Pd, Fe and Au samples. A scan of Ag NP was not performed as its chemical reduction on PEI was demonstrated successfully previously by an XRD of Ag NP[3]. Of the other metals tested, the Cu sample was the only catalyst to show a peak as displayed in Figure 4B. This was likely due to the other metals being at a surface density too low to be detected, as indicated in Table 2, and the signal produced too weak to

overcome the background noise of the PEI signal, rather than the samples being amorphous. The peak on the Cu sample was measured at  $43.2^\circ$  which coincides with the crystallographic plane of Cu (111)[63]. The Cu sample displayed monocrystalline behaviour due to the sharpness of the peak detected [64]. Other peaks expected for Cu at  $50.4^\circ$  (200) and  $74.1^\circ$  (220) were not detectable outside of the noise of the XRD pattern. The average crystalline size can be approximated for the NPs using equation  $D \approx \frac{K\lambda}{\beta \cos \theta}$  (1)

and the conditions,  $\beta = 0.06^\circ$  (evaluated as the full width half maximum of the peak) and  $\theta = 43.2/2 = 21.6^\circ$  (the Cu (111) peak's angle), to give a D value for the Cu peak of  $14 \pm 3$  nm. This value is similar to the average particle size measured from SEM analysis,  $30 \pm 15$  nm, as shown in Table 2.

The elements Cu, Ag and Fe are clearly identified using UV-Vis spectroscopy and XRD[3]. The remaining elements listed in Table 2 were identified from EDX scans. The Au sample shows a low percentage of the metal in its surface which correlates with the low particle density measured. Under certain conditions of mixing, temperature and concentration, metal-boride NP can form for the metals used in this study, when chemically reduced with reducing agent  $\text{NaBH}_4$  [65]. Boron signal counts were not detected in the EDX or XPS scans of the metal surfaces, indicating that either they did not form, were in a concentration too low to be detected, or their peaks overlapped with other elements. Under the processing conditions applied in the study, it is likely that these were unfavourable for metal-boride NP formation.

FTIR scans were also performed on the different surfaces as shown in Figure 4C. Absorption peaks were more pronounced for higher particle densities. Medium sized peaks were observed on the Cu sample around  $1652 \text{ cm}^{-1}$  and  $1557 \text{ cm}^{-1}$ . These are attributed to amide I and II vibrations accordingly, which are formed after hydrolysis and onto which the metal ions bond. Their presence for the different metal scans indicates the binding of metal ions to the PEI. A weak peak is observed around  $1418 \text{ cm}^{-1}$  after metal reduction, indicating the presence of C=C bond stretching within a carboxyl group, attributed to the presence of metal ion bonds in the PEI[5,66]. Hydrolysis of the PEI involves imide ring cleavage. This is indicated by a reduction in size between the untreated PEI and the metal bound PEI of the C=O symmetric imide peak at  $1716 \text{ cm}^{-1}$ . The presence of this peak after metal reduction indicates that complete breaking of all imide rings did not occur and that more aggressive hydrolysis could be performed[3].

Photoreduction of embedded Ag ions in PEI was successfully demonstrated in a previously published method[5]. In this article photoreduction was monitored using FTIR, as

the reduction in peak-size of imide functional groups and the formation of amide groups on the PEI surface after photoreduction, as also witnessed in Figure 4C after chemical reduction of the ions. This photoreduction method was applied with the same settings in the current study for the different ion exchanged metals, to try to achieve selective circuitry formation using other metal catalysts. Other than Ag, none of the other metal ions successfully photoreduced onto PEI under the parameters tested as evidenced by optical microscopy, XRD or subsequent electroless Cu plating. The reason for this behaviour could be due to the ion exchange of  $\text{Cl}^-$  from KCl with the  $m^+$  on the hydrolysed PEI surface forming  $m\text{Cl}$ . For Ag, the formation of AgCl halide salt on PEI is identified as the compound responsible for increased photoreduction rates when processing [5]. Increases to the density of the Ag NP film formed after photoreduction was witnessed on prolonged exposure to KCl, indicating the interdependence of KCl ion exchange on Ag photoreduction rate. Additionally, SEM images of PEI surface in [5] showed that for the processing settings applied, no Ag NP were witnessed on the surface of the PEI without KCl treatment. The formation of  $m\text{Cl}$  was not observed with the other metals on the PEI surface using UV-Vis spectroscopy or XRD techniques. Another factor to consider is the different degrees of photosensitivity of  $m\text{Cl}$  salts from different metals[67–69]. If the  $m\text{Cl}$  salts were formed on the PEI surface but at a concentration too low to be detected by the techniques applied, then it is also not clear whether they will photoreduce as readily as AgCl, under the conditions tested. The concentration of optical sensitizers has been shown to influence the rate of photoreduction, as demonstrated in the photoreduction of Cu using formic acid [36]. Changes to the applied KCl concentrations, prior to photoreduction for the different metal ions, may alter and improve their photoreduction performance.

The power and duration of the applied light influences the photoreduction performance [68], where increases to exposure duration increase the degree of photoreduction [5]. For the different metal catalysts, longer exposure durations and different optical powers may change the photoreduction performance, although greater increases to optical power could induce unwanted damage to the PEI substrate.

Another parameter influencing photoreduction performance is the exposure wavelength, since values closer to the localized surface plasmon resonance of the growing metallic NP show improved optical absorbance and increase photoreduction rates, as demonstrated for Ag NP in [5]. Tuning the wavelength of optical exposure to the resonant values predicted for the different metal NPs could improve photoreduction rates. The resonant frequencies for the different metals are approximately: Ag 420 nm[70]; Au 540 nm[70]; Cu

610 nm[71,72]; Ni 350 nm[73]; Fe 260 nm[53]; and Pd 280 nm[74], although the optimum wavelength depends on the size of the NP and their morphology.

### 3.2 Quality of the electroless copper deposit

The PEI surfaces, activated by ion exchange of the metal catalysts and their chemical reduction, were electroless Cu plated using the same process duration and bath formulation. On the samples which plated successfully, measures of Cu thickness were obtained from cross-sectional surface profiles using Dektak equipment, as shown in Figure 5. In A, electroless Cu deposit formed on Ag NP coated PEI, was characterised over a 1000  $\mu\text{m}$  line and displayed an average arithmetic roughness (Ra) of  $50 \pm 10$  nm, that coincided with a densely packed Cu deposit [5]. In B, the deposited Cu thickness was measured from a 150  $\mu\text{m}$  line scan over the edge of the Cu deposit and the PEI substrate, which was approximately 0.8  $\mu\text{m}$ . Deposited thickness matched with values previously obtained for the plating settings applied [5].

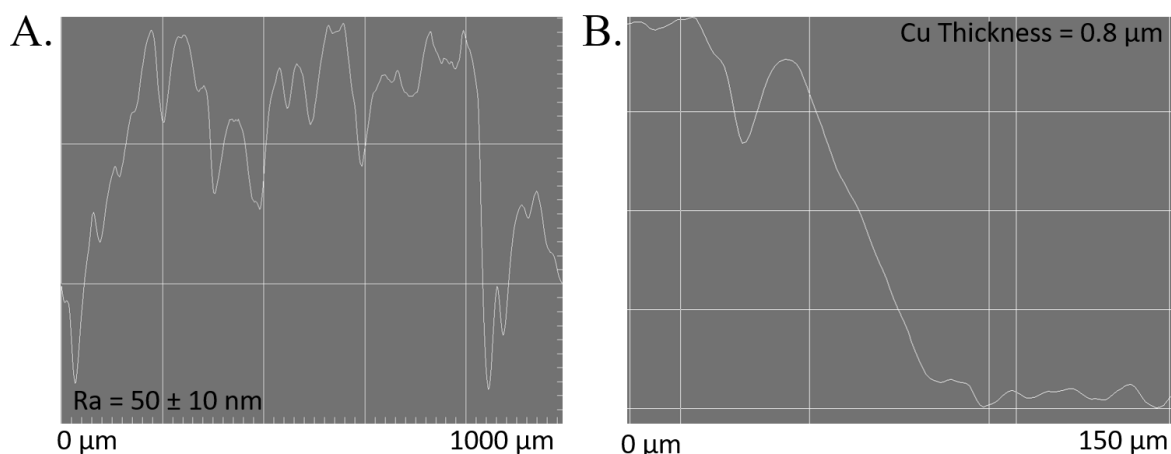




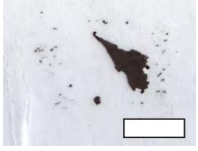
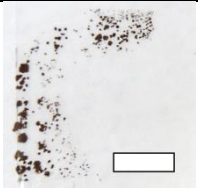
Figure 5 – Dektak cross-section profile of electroless Cu plated onto Ag NP chemically reduced PEI surfaces, A) 1000  $\mu\text{m}$  section of Cu surface and B) Edge of Cu plated region.

Using values for Cu thickness and electrical resistance, plating rate and conductivity were evaluated, as displayed in Table 3. The measured plating rates varied from 1.3 to 2.4  $\mu\text{m/hr}$  and are comparable with typical plating rates obtained for electroless Cu plating in PCB manufacture, which is approximately 2  $\mu\text{m/hr}$ [75]. The fastest plating rates were measured with Cu and Pd catalysts and coincide with high catalytic activity[17] and particle density as shown in Table 2. The conductivity of the Cu deposits all were within a factor of 10 of the value for bulk Cu ( $5.96 \times 10^7$  S/m), which is comparable to values expected for the thicknesses measured[75]. The pH of the electroless Cu solution was measured before and after each plating cycle, for the different metal catalysts. For all samples the initial average pH was


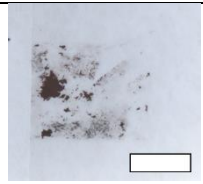
measured as  $12.4 \pm 0.5$  and did not vary outside of this range after each plating. This was in-line with expected pH values for the electroless Cu formulation used [76].

The adhesion of the electroless Cu deposit was assessed using Scotch tape test standard (IPC. IPC-TM-650)[41]. The absence of Cu present on the tape after its removal, was only witnessed for Cu and Ag catalysts as indicated in Table 3. The Cu and Ag NPs formed the highest uniformity when reduced on the PEI surface, as indicated in Table 2. As such, these seed layers could have displayed the lowest inter-pore spacing in the plated Cu and a higher ductility. Additionally, Ag catalyst produces a high adhesion with electroless Cu plating when compared with Pd[77] and so its successful adhesion here is unsurprising. The Pd and Au catalysts show a poor adhesion despite their high catalytic activities. Reasons for this could be the shallow depth of the Pd absorbed into the PEI surface due to its shorter ion exchange processing duration (5 min rather than 60 min), and lower ion exchange solution processing temperature of 20°C rather than 50°C.

*Table 3 – Electroless Cu deposit quality in terms of conductivity and adhesion strength onto PEI. The scale bar shown has a length of 1 cm.*

<b>Metal catalyst</b>	<b>Electroless copper plating rate (<math>\pm 0.1 \mu\text{m/hr}</math>)</b>	<b>Electroless copper Conductivity (<math>\times 10^7 \text{ S/m}</math>)</b>	<b>Tape test (scale 1 cm)</b>	
<b>Silver nitrate</b>	1.5	$3.6 \pm 0.2$	Pass	
<b>Copper sulphate</b>	2.3	$2.0 \pm 0.5$	Pass	
<b>Nickel chloride</b>	1.3	$1.9 \pm 0.2$	Fail	
<b>Gold chloride</b>	1.7	$2.0 \pm 0.5$	Fail	



<b>Palladium chloride</b>	2.3	$2.5 \pm 0.5$	Fail	
<b>Iron sulphate</b>	1.4	$3.0 \pm 0.5$	Fail	

The Au particle density was low on the PEI surface leading to lower numbers of active sites to bind to, which could explain its weaker adhesion. Increases of Gold (III) chloride trihydrate concentration or solution temperature during ion exchange could improve ion exchange performance, although the former is a less economic solution. The poor adhesion witnessed on the Fe catalysts could be due to its ability to readily oxidise, and thus presents an unsatisfactory surface to plate onto[55]. Fe NP formed by chemical reduction oxidise under air after several seconds [53]. Addition of an acid or electron beam etch before plating could help to remove the Fe oxide, although this would risk reducing the density of the Fe nanoparticle layer[17,52]. Additionally, oxidation could be reduced by performing the Fe chemical reduction under vacuum or in an inert atmosphere such as argon or nitrogen [53]. The Ni shows a poor Cu adhesion as the NPs deposited show large clusters formation on the surface, as shown in Figure 3C. The large gaps between the Ni clusters, are likely to have been carried forwards into the plated Cu grain structure resulting in a weak deposit[56]. Improvements to adhesion could be made by reducing the Ni reduction time, temperature or bath concentration, and thus promoting the formation of smaller Ni deposits of a higher surface density and smaller gaps.

### 3.3 Inclusion of a H<sub>2</sub>SO<sub>4</sub> acid pre-treatment

The inclusion of a H<sub>2</sub>SO<sub>4</sub> pre-treatment before KOH pre-treatment on PEI is known to improve the adhesion of electroless Cu deposits to the PEI surface[66]. The treatment increases sulphuric oxidation on the PEI surface and increases wettability, which when electroless Cu plated, demonstrates increased peel strength values [78]. The incorporation of H<sub>2</sub>SO<sub>4</sub> pre-treatment can be applied to both chemical reduction and photoreduction procedures. Here it is applied to photoreduction. Figure 6 shows the high-resolution images of the PEI surfaces after selective Ag photoreduction (A and B) and electroless Cu plating (C and D), with SEM inserts of the Ag NPs after photoreduction. The width of the central track feature is 150 μm, with feature resolution limited by size of optical mask used for exposure. Images were obtained with the same contrast settings and scratches observed on the surface are due to handling. With pre-

treatment including H<sub>2</sub>SO<sub>4</sub>, photoreduction appears with greater density highlighted by the yellow shade of the Ag metal nanoparticles[79] against the blue background of the un-reduced PEI surface. The SEM images of the photoreduced surfaces show greater particle densities (3.5 counts/ $\mu\text{m}^2$ ) with H<sub>2</sub>SO<sub>4</sub> treatment than without (0.5 counts/ $\mu\text{m}^2$ ). Measures of the SEM cross-section of the Ag NPs on the PEI for both samples showed an average thickness of  $120 \pm 30$  nm and  $150 \pm 40$  nm, respectively. There was no noticeable difference in thickness between the two samples and the resolution of the features was low, which was likely influenced by sample preparation and image drift.

The electroless plating rate was calculated by measuring the Cu thickness for both pre-treated electroless plated samples. Plating rate was  $0.9 \pm 0.1$   $\mu\text{m/hr}$  for H<sub>2</sub>SO<sub>4</sub> followed by KOH and  $0.3 \pm 0.1$   $\mu\text{m/hr}$  for KOH only. A greater uptake of Ag ions occurs into the PEI with H<sub>2</sub>SO<sub>4</sub>, providing greater numbers of active sites for photoreduction and plating. With H<sub>2</sub>SO<sub>4</sub> pre-treatment, electroless Cu conductivity is  $(2.5 \pm 0.5) \times 10^7$  S/m and passes the tape test. Without H<sub>2</sub>SO<sub>4</sub>, the area exposed by UV light did not produce a sufficient density of NPs to produce a conductive electroless Cu deposit for the time plated. The sample also did not pass the tape test.

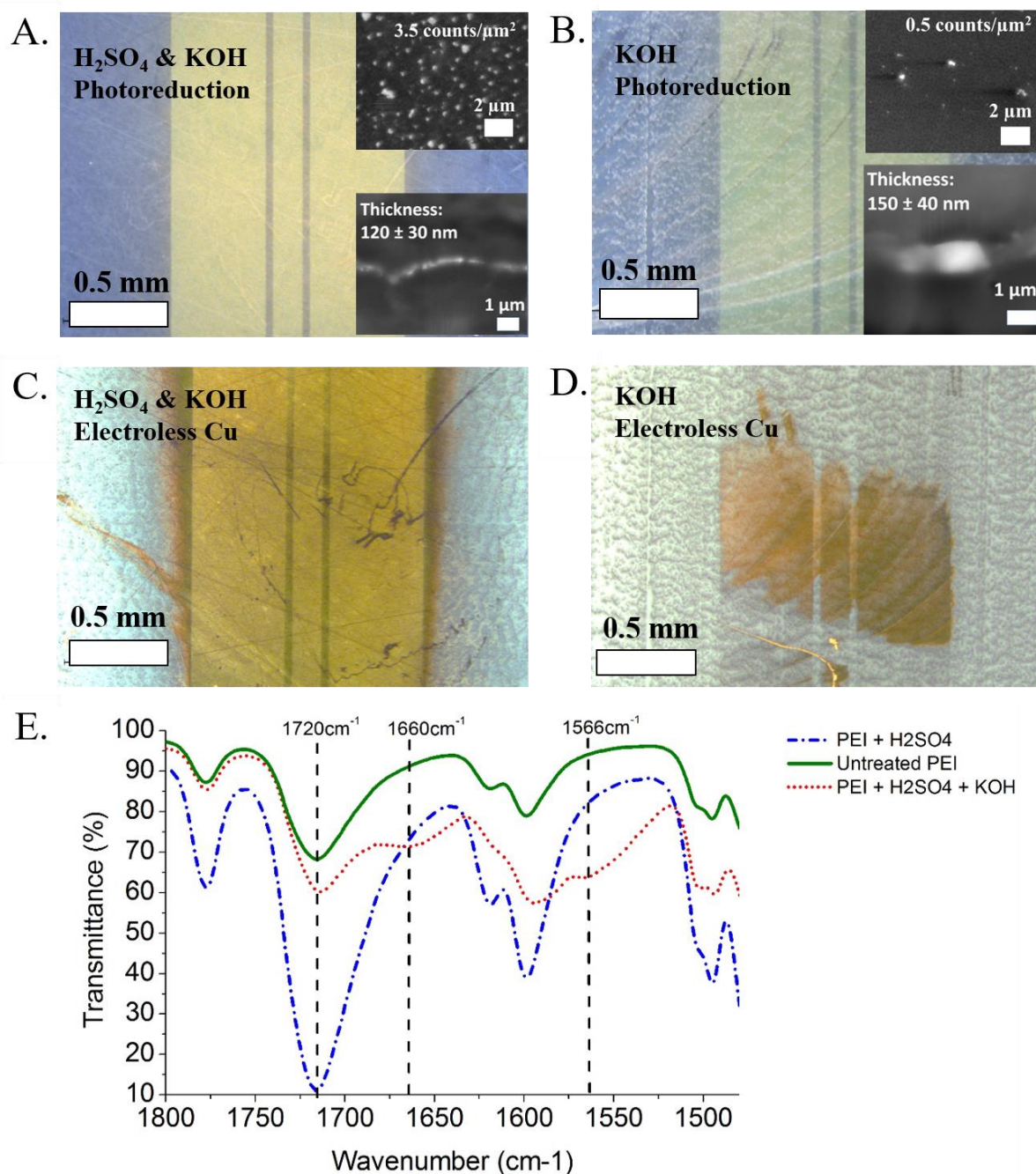


Figure 6 – PEI surfaces with pre-treatments H<sub>2</sub>SO<sub>4</sub> and KOH A) & C), and only KOH B) & D); after photoreduction A) & B), and after electroless plating C) & D). SEM inserts included alongside photoreduced samples A) & B) of surface and cross-section. E) FTIR spectra for PEI surfaces with different pre-treatments.

FTIR was performed on the PEI films treated with H<sub>2</sub>SO<sub>4</sub> and H<sub>2</sub>SO<sub>4</sub> followed by KOH. The results are displayed in a plot in Figure 6E and show that, with H<sub>2</sub>SO<sub>4</sub>, no new absorption peaks were detected. Appearance of the 1720 cm<sup>-1</sup> peak indicates the presence of the carboxylic acid group, which contributes to the increase of the ion exchange of metal ions[5,66]. With the

inclusion of KOH, the breaking of imide peaks to form amide peaks is observed, as reported in Figure 4.

### 3.4 Influence of KCl concentration on photoreduction performance

Studies were performed to identify the minimum KCl concentration required to photoreduce the Ag catalysts with a high NP density. Figure 7A presents the UV-Vis absorption spectra for Ag NPs on PEI surfaces photoreduced with different concentrations of KCl under the same optical settings.

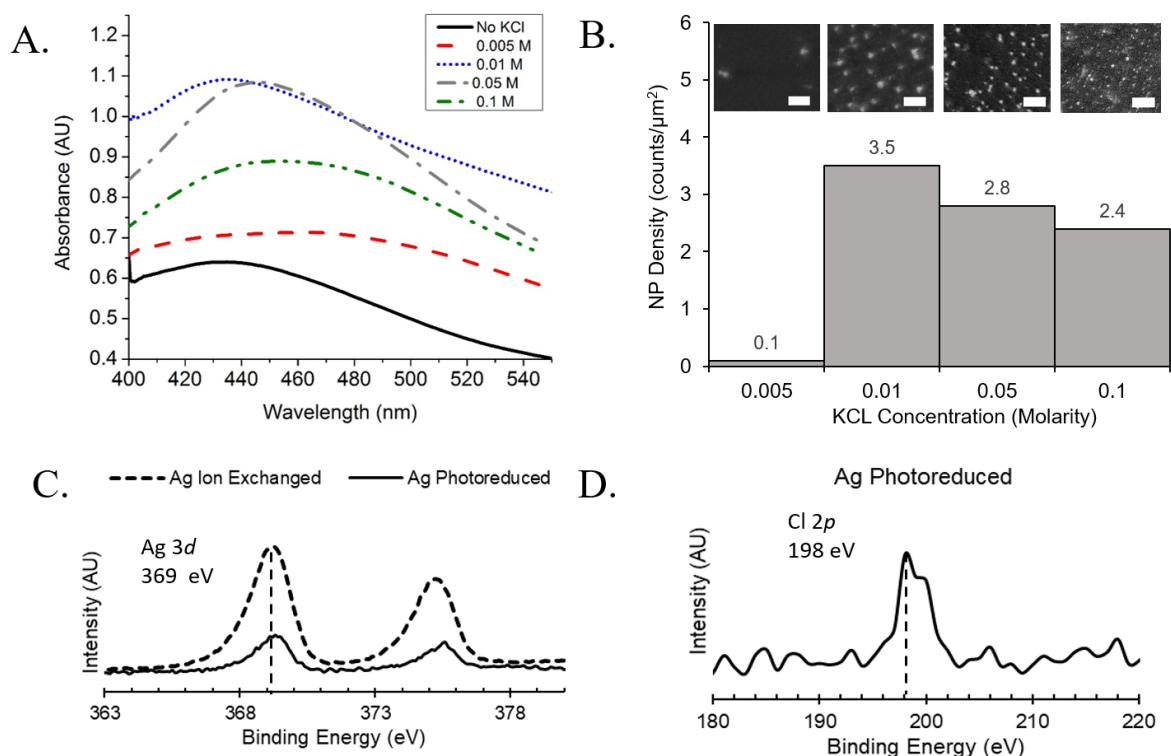


Figure 7 – A) UV-Vis absorbance spectroscopy for Ag NP formed after photoreduction for different concentrations of KCl. B) Plot of NP density against KCl concentration with insert SEM images of NP on surface, scale 1  $\mu\text{m}$ . XPS of C) Ag ion exchanged PEI and Ag photoreduced PEI, and D) Ag photoreduced PEI.

The higher peaks correspond to larger densities of photoreduced Ag NPs[62]. The highest peak was obtained for an optimum concentration 0.01 M, with higher or lower concentrations resulting in lower peaks and thus smaller particle densities on the PEI surface. Without KCl, a small peak was obtained indicating the weakest photoreduction of Ag ions. Plots of NP density at different KCl concentrations are shown in Figure 7B with inserts of corresponding SEM images of the PEI surfaces after photoreduction. The plot highlights again that the largest particle density is obtained for 0.01 M KCl. The results show that the

photoreduction rate is influenced by the application of KCl. KCl enables the formation of photosensitive AgCl [5] and without its application, the Ag ions present on the PEI surface are less photosensitive, which in turn induces less photoreduction to Ag metal.

For KCl concentrations increasing up to 0.01 M, the amount of AgCl salt formed on the PEI surface increases, enabling increased numbers of active sites for photoreduction and thus larger NP densities for same duration exposed[36]. Beyond 0.01 M, the drop in Ag photoreduced NP density observed at higher concentrations could be due to unwanted scattering of light on the surface of the PEI caused by the excess Ag NPs produced during photoreduction at high KCl concentrations. The increased numbers of Ag NP on the surface could prevent penetration of light into the PEI, reducing the overall photon flux absorption and photoreduction of NPs within the PEI on the surface, as observed in other photocatalyst systems[80–82]. The SEM inserts in Figure 7B highlight NP formed several microns into the PEI substrate as well as on its surface and so, the reductions in NP density measured at higher KCl concentrations could reflect reductions to NPs formed inside of the PEI rather than on its surface.

Highlighted in Figure 7C is XPS measures of Ag photo-exposed on PEI using 0.01 M KCl showing Ag 3d peak at ~369.0 eV, which is attributed to Ag metal [44], as also witnessed after Ag chemical reduction, see Figure 2. Shown in Figure 7D is a Cl 2p peak at 198 eV [83] in the spectrum of the photoreduced PEI, which is present due to the formation of AgCl. The presence of the Ag metal peak highlight photoreduction of the Ag ions to Ag metal[5,83].

## 4 Conclusions

Ion exchange and chemical reduction have been demonstrated onto PEI by a range of metal catalysts commonly used in electronics manufacture. The successful demonstration of the reduction of the metal ions onto PEI plastic enables their use in a wide range of electronics applications. High quality electroless Cu deposition was obtained with economic catalysts Ag and Cu enabling reduced fabrication costs.

KCl enhanced photoreduction was not observed on metal catalysts other than Ag using the parameters tested. An optimum KCl concentration required for the photoreduction of Ag<sup>+</sup> using KCl sensitizer was also demonstrated. Improvements to the formation of direct metallised tracks was obtained in terms of electroless Cu plating rate and adhesion and Ag<sup>+</sup> photoreduction rate, by the inclusion of H<sub>2</sub>SO<sub>4</sub> prior to plating. The underlying improvements are attributed to increased metal ion uptake onto the PEI surface, improving photoreduction.

The improvements obtained allow for reductions to processing costs and if applied within manufacture reduces turnover.

## Acknowledgements

The authors thank the Engineering & Physical Sciences Research Council (EPSRC) for their financial support under the grants Photobioform I (Grant Nos. EP/L022192/1 and EP/L022133/1) and Photobioform II (Grant Nos. EP/N018222/1 and EP/N018265/2). We would also like to especially thank Dr. Beth Willneff and support from the Henry Royce Institute (EPSRC grants: EP/P022464/1, EP/R00661X/1), which funded the VXSF Facilities (<https://engineering.leeds.ac.uk/vxsf>) within the Bragg Centre for Materials Research at Leeds and Dr. Jim Buckman at Heriot-Watt University, UK, for electron microscopy.

## References

- [1] Polyimide Films Market (Application - Wires and Cables Insulation, Flexible PCB, Labels, and Barcode) - Global Industry Analysis, Size, Share, Growth, Trends and Forecast 2016 - 2024, (2016).
- [2] D.J. Kemmish, High Performance Engineering Plastics, Rapra Technology Limited, 1995.
- [3] D.E. Watson, J.H.G. Ng, K.E. Aasmundtveit, M.P.Y. Desmulliez, In-Situ Silver Nanoparticle Formation on Surface-Modified Polyetherimide Films, *IEEE Trans. Nanotechnol.* 13 (2014) 736–742. doi:10.1109/TNANO.2014.2318203.
- [4] T.D.A. Jones, A. Ryspayeva, M.N. Esfahani, R.A. Harris, R.W. Kay, J. Marques-Hueso, M.P.Y. Desmulliez, Direct metallisation method onto 3-D printed polyetherimide substrates, *Innov. Large-Area Electron. Conf. 2018* . (2018) 100–101.
- [5] J. Marques-Hueso, T.D.A. Jones, D.E. Watson, A. Ryspayeva, M.N. Esfahani, M.P. Shuttleworth, R.A. Harris, R.W. Kay, M.P.Y. Desmulliez, A Rapid Photopatterning Method for Selective Plating of 2D and 3D Microcircuitry on Polyetherimide, *Adv. Funct. Mater.* 28 (2018) 1–8. doi:DOI: 10.1002/adfm.201704451.
- [6] M.P.Y. Desmulliez, D.E. Watson, J. Marques-Hueso, J.H.-G. Ng, N.F. Lepora, A. Mura, M. Mangan, P.F.M.J. Verschure, M. Desmulliez, T.J. Prescott, A Bio-Inspired Photopatterning Method to Deposit Silver Nanoparticles onto Non Conductive Surfaces Using Spinach Leaves Extract in Ethanol, *Biomim. Biohybrid Syst. Living Mach.* 2016. 9793 (2016) 71–78. doi:[https://doi.org/10.1007/978-3-319-42417-0\\_7](https://doi.org/10.1007/978-3-319-42417-0_7).

- [7] J. Marques-Hueso, R. Abargues, J.L. Valdes, J.P. Martinez-Pastor, Ag and Au/DNQ-novolac nanocomposites patternable by ultraviolet lithography: a fast route to plasmonic sensor microfabrication, *J. Mater. Chem.* 20 (2010) 7436–7443. doi:10.1039/C0JM01226B.
- [8] J. Marques-Hueso, J.A.S. Morton, X. Wang, E. Bertran-Serra, D. M P Y, Photolithographic nanoseeding method for selective synthesis of metal-catalysed nanostructures, *Nanotechnology.* 30 (2019) 15302. <http://stacks.iop.org/0957-4484/30/i=1/a=015302>.
- [9] D.E. Watson, J.H.G. Ng, M.P.Y. Desmulliez, Additive photolithography based process for metal patterning using chemical reduction on surface modified polyimide, in: *Microelectron. Packag. Conf. (EMPC), 2011 18th Eur.*, 2011: pp. 1–7.
- [10] J. Marques-Hueso, R. Abargues, J. Canet-Ferrer, J.L. Valdes, J. Martinez-Pastor, Resist-based silver nanocomposites synthesized by lithographic methods, *Microelectron. Eng.* 87 (2010) 1147–1149. doi:<https://doi.org/10.1016/j.mee.2009.10.043>.
- [11] J. Marqués-Hueso, R. Abargues, J. Canet-Ferrer, S. Agouram, J.L. Valdés, J.P. Martínez-Pastor, Au-PVA Nanocomposite Negative Resist for One-Step Three-Dimensional e-Beam Lithography, *Langmuir.* 26 (2010) 2825–2830. doi:10.1021/la902915n.
- [12] K. Akamatsu, S. Ikeda, H. Nawafune, H. Yanagimoto, Direct Patterning of Copper on Polyimide Using Ion Exchangeable Surface Templates Generated by Site-Selective Surface Modification, *J. Am. Chem. Soc.* 126 (2004) 10822–10823. doi:10.1021/ja047700e.
- [13] Y. Matsumura, Y. Enomoto, M. Sugiyama, K. Akamatsu, H. Nawafune, Direct metallization of nickel on polymeric template patterns for fabrication of copper circuits on glass substrates, *J. Mater. Chem.* 18 (2008) 5078–5082. doi:10.1039/B808267G.
- [14] V.F. Kiselev, O. V Krylov, *Adsorption and Catalysis on Transition Metals and Their Oxides*, Springer Berlin Heidelberg, 2012.
- [15] K.L. Mittal, *Polyimides and Other High Temperature Polymers: Synthesis, Characterization and Applications*, CRC Press, 2007.
- [16] M. Seita, H. Nawafune, T. Nishioka, S. Mizumoto, T. Kanai, Photochemical formation of palladium patterns on surface-modified polyimide resin, *J. Appl. Electrochem.* 32 (2002) 349–352. doi:10.1023/a:1015554625106.
- [17] G.A. Krulik, Tin-Palladium Catalysts for Electroless Plating, *Platinum Met. Rev.* 26 (1982) 58–64.

- [18] Xiaoyun Cui, David. A. Hutt, David. J. Scurr, P.P. Conway, The evolution of Pd/Sn catalytic surfaces in electroless copper deposition, *J. Electrochem. Soc.* 158 (2011) D172–D177.
- [19] Z.-C. Liu, Q.-G. He, P. Hou, P.-F. Xiao, N.-Y. He, Z.-H. Lu, Electroless plating of copper through successive pretreatment with silane and colloidal silver, *Colloids Surfaces A Physicochem. Eng. Asp.* 257–258 (2005) 283–286. doi:<http://dx.doi.org/10.1016/j.colsurfa.2004.10.036>.
- [20] S.-E. Huang, W.-P. Dow, Influence of reducibility of reductant on nickel nanoparticles formation on polyimide, in: 2010 5th Int. Microsystems Packag. Assem. Circuits Technol. Conf., IEEE, Taipei, Taiwan, 2010: pp. 1–4. doi:10.1109/IMPACT.2010.5699514.
- [21] G. Cui, W. Liu, L. Yuan, D. Wu, Z. Wu, Transition of polyimide/[small alpha]-Fe<sub>2</sub>O<sub>3</sub> to polyimide/Fe<sub>3</sub>O<sub>4</sub> nanocomposite films by adjusting thermal treatment surroundings of ion-doped substrates, *RSC Adv.* 3 (2013) 14390–14396. doi:10.1039/C3RA41461B.
- [22] S. Mu, Z. Wu, Y. Wang, S. Qi, X. Yang, D. Wu, Formation and characterization of cobalt oxide layers on polyimide films via surface modification and ion-exchange technique, *Thin Solid Films.* 518 (2010) 4175–4182. doi:<https://doi.org/10.1016/j.tsf.2009.12.004>.
- [23] N.S. Yousef, R. Hazzaa, R. Farouq, Adsorptive Removal of Chromium (III) from Aqueous Solution Using Cation-Exchange Resin: Development of an Empirical Model, *Int. Proc. Chem. Biol. Environ. Eng.* 88 (2015) 21–29.
- [24] M.A. Mohiddon, K.L. Naidu, M.G. Krishna, G. Dalba, S.I. Ahmed, F. Rocca, Chromium oxide as a metal diffusion barrier layer: An x-ray absorption fine structure spectroscopy study, *J. Appl. Phys.* 115 (2014) 44315. doi:10.1063/1.4863309.
- [25] S.H. Cho, S.H. Kim, J.G. Lee, N.E. Lee, Micro-scale metallization of high aspect-ratio Cu and Au lines on flexible polyimide substrate by electroplating using SU-8 photoresist mask, *Microelectron. Eng.* 77 (2005) 116–124. doi:<https://doi.org/10.1016/j.mee.2004.09.007>.
- [26] B. Ankamwar, T.C. Lai, J.H. Huang, R.S. Liu, M. Hsiao, C.H. Chen, Y.K. Hwu, Biocompatibility of Fe<sub>3</sub>O<sub>4</sub> nanoparticles evaluated by in vitro cytotoxicity assays using normal, glia and breast cancer cells, *Nanotechnology.* 21 (2010) 75102. doi:<https://doi.org/10.1088/0957-4484/21/7/075102>.
- [27] F. Faupel, R. Willecke, A. Thran, Diffusion of metals in polymers, *Mater. Sci. Eng. R Reports.* 22 (1998) 1–55. doi:[https://doi.org/10.1016/S0927-796X\(97\)00020-X](https://doi.org/10.1016/S0927-796X(97)00020-X).



- [28] V. Iyer, J. Chan, S. Gollakota, 3D printing wireless connected objects, *ACM Trans. Graph.* 36 (2017) 1–13. doi:10.1145/3130800.3130822.
- [29] J. Faerber, G. Cummins, S.K. Pavuluri, P. Record, A.R.A. Rodriguez, H.S. Lay, R. McPhillips, B.F. Cox, C. Connor, R. Gregson, R.E. Clutton, S.R. Khan, S. Cochran, M.P.Y. Desmulliez, In Vivo Characterization of a Wireless Telemetry Module for a Capsule Endoscopy System Utilizing a Conformal Antenna, *IEEE Trans. Biomed. Circuits Syst. PP* (2017) 1–11. doi:10.1109/TBCAS.2017.2759254.
- [30] G. Schiavone, T. Jones, D. Price, R. M, Y. Jiang, Z. Qiu, C. Meggs, S.O. Mahboob, S. Eljamel, W.T. Button, C.E.M. Demore, S. Cochran, M.P.Y. Desmulliez, A highly compact packaging concept for ultrasound transducer arrays embedded in neurosurgical needles, *Springer, Microsystems Technol.* 22 (2015) 1–11. doi:https://doi.org/10.1007/s00542-015-2775-1.
- [31] M.R.N. Esfahani, M.P. Shuttleworth, R.A. Harris, R.W. Kay, V. Doychinov, I.D. Robertson, J. Marques-Hueso, T.D.A. Jones, A. Ryspayeva, M.P.Y. Desmulliez, Hybrid Additive Manufacture of Conformal Antennas, in: 2018 IEEE MTT-S Int. Microw. Work. Ser. Adv. Mater. Process. RF THz Appl., 2018: pp. 1–3. doi:10.1109/IMWS-AMP.2018.8457128.
- [32] A. Ryspayeva, T.D.A. Jones, P.A. Hughes, R.A.H. M.N. Esfahani, M.P.Shuttleworth, R.W. Kay, M.P.Y. Desmulliez, J. Marques-Hueso, PEI/Ag as an optical gas nano-sensor for intelligent food packaging, in: 2018 IEEE Int. Conf. Nanotechnol., Cork, Ireland
- [33] H. Kim, Y.S. Seo, K. Kim, J.W. Han, Y. Park, S. Cho, Concentration Effect of Reducing Agents on Green Synthesis of Gold Nanoparticles: Size, Morphology, and Growth Mechanism, *Nanoscale Res. Lett.* 11 (2016) 230. doi:10.1186/s11671-016-1393-x.
- [34] T.D.A. Jones, A. Bernassau, D. Flynn, D. Price, M. Beadel, M.P.Y. Desmulliez, Copper electroplating of PCB interconnects using megasonic acoustic streaming, *Ultrason. Sonochem.* 42 (2018) 434–444. doi:https://doi.org/10.1016/j.ultsonch.2017.12.004.
- [35] T.D.A. Jones, D. Flynn, M.P.Y. Desmulliez, D. Price, M. Beadel, N. Strusevich, M. Patel, C. Bailey, S. Costello, T.D.A. Jones, D. Flynn, M.P.Y. Desmulliez, D. Price, M. Beadel, N. Strusevich, M. Patel, C. Bailey, S. Costello, Morphology and acoustic artefacts of copper deposits electroplated using megasonic assisted agitation, *Circuit World.* 42 (2016) 127–140. doi:10.1108/CW-03-2016-0006.
- [36] M. Canterino, I. Di Somma, R. Marotta, R. Andreozzi, Kinetic investigation of Cu(II) ions photoreduction in presence of titanium dioxide and formic acid, *Water Res.* 42 (2008) 4498–4506. doi:https://doi.org/10.1016/j.watres.2008.07.035.

- [37] Y. Kong, J. Shao, W. Wang, Z. Chen, H. Chu, Surface modification and metallization of polyimide using gold colloids as a seed layer, *J. Appl. Polym. Sci.* 111 (2009) 2044–2048. doi:10.1002/app.29188.
- [38] S.S. Yoon, D.O. Kim, S.C. Park, Y.K. Lee, H.Y. Chae, S.B. Jung, J.D. Nam, Direct metallization of gold patterns on polyimide substrate by microcontact printing and selective surface modification, *Microelectron. Eng.* 85 (2008) 136–142. doi:https://doi.org/10.1016/j.mee.2007.04.142.
- [39] F.T. Stepto Robert, Dispersity in polymer science (IUPAC Recommendations 2009), *Pure Appl. Chem.* 81 (2009) 351. doi:10.1351/PAC-REC-08-05-02.
- [40] A. Nematollahzadeh, M.J. Abdekhodaie, A. Shojaei, Submicron nanoporous polyacrylamide beads with tunable size for verapamil imprinting, *J. Appl. Polym. Sci.* 125 (2012) 189–199. doi:10.1002/app.35426.
- [41] IPC, IPC-TM-650 Test Methods Manual, 2.6.8. (n.d.). <https://www.ipc.org/test-methods.aspx>.
- [42] M.C. Burrell, J.J. Chera, Polyetherimide (Ultem®) Spin Cast Films by XPS, *Surf. Sci. Spectra.* 6 (1999) 18–22. doi:10.1116/1.1247898.
- [43] A.M. Ferraria, A.P. Carapeto, A.M. Botelho do Rego, X-ray photoelectron spectroscopy: Silver salts revisited, *Vacuum.* 86 (2012) 1988–1991. doi:https://doi.org/10.1016/j.vacuum.2012.05.031.
- [44] S.C.V. and R.E.G. and N.B. and C.P. and A.C. and S. Carvalho, Ag + release inhibition from ZrCN–Ag coatings by surface agglomeration mechanism: structural characterization, *J. Phys. D. Appl. Phys.* 46 (2013) 325303. <http://stacks.iop.org/0022-3727/46/i=32/a=325303>.
- [45] Y. Liu, P. Bailey, T.C.Q. Noakes, G.E. Thompson, P. Skeldon, M.R. Alexander, Chemical environment of copper at the surface of a CuAl<sub>2</sub> model alloy: XPS, MEIS and TEM analyses, *Surf. Interface Anal.* 36 (2004) 339–346. doi:10.1002/sia.1743.
- [46] N. Hackerman, E. McCafferty, R.J. Brodd, E.S.C. Division, Surfaces, Inhibition, and Passivation: Proceedings of an International Symposium Honoring Doctor Norman Hackerman on His Seventy-fifth Birthday, Corrosion Division, Electrochemical Society, 1986.
- [47] Y.-H. Tseng, B.-K. Huang, Photocatalytic Degradation of NO<sub>x</sub> Using Ni-Containing TiO<sub>2</sub>, *Int. J. Photoenergy.* 2012 (2012) 7. doi:10.1155/2012/832180.
- [48] M.C. Militello, S.J. Simko, Palladium Chloride (PdCl<sub>2</sub>) by XPS, *Surf. Sci. Spectra.* 3 (1994) 402–409. doi:10.1116/1.1247785.

- [49] E. Ismail, M. Khenfouch, M. Dhlamini, S. Dube, M. Maaza, Green palladium and palladium oxide nanoparticles synthesized via *Aspalathus linearis* natural extract, *J. Alloys Compd.* 695 (2017) 3632–3638. doi:<https://doi.org/10.1016/j.jallcom.2016.11.390>.
- [50] H.-F. Li, N. Zhang, P. Chen, M.-F. Luo, J.-Q. Lu, High surface area Au/CeO<sub>2</sub> catalysts for low temperature formaldehyde oxidation, *Appl. Catal. B Environ.* 110 (2011) 279–285. doi:<https://doi.org/10.1016/j.apcatb.2011.09.013>.
- [51] Y. Ishida, I. Akita, T. Sumi, M. Matsubara, T. Yonezawa, Thiolate-Protected Gold Nanoparticles Via Physical Approach: Unusual Structural and Photophysical Characteristics, *Sci. Rep.* 6 (2016) 29928. <https://doi.org/10.1038/srep29928>.
- [52] K.-C. Huang, S.H. Ehrman, Synthesis of Iron Nanoparticles via Chemical Reduction with Palladium Ion Seeds, *Langmuir.* 23 (2007) 1419–1426. doi:10.1021/la0618364.
- [53] K. Klačanová, P. Fodran, P. Šimon, P. Rapta, R. Boča, V. Jorík, M. Miglierini, E. Kolek, L. Čaplovič, Formation of Fe(0)-Nanoparticles via Reduction of Fe(II) Compounds by Amino Acids and Their Subsequent Oxidation to Iron Oxides, *J. Chem.* 2013 (2013) 10. doi:10.1155/2013/961629.
- [54] R.W.J. Scott, H. Ye, R.R. Henriquez, R.M. Crooks, Synthesis, Characterization, and Stability of Dendrimer-Encapsulated Palladium Nanoparticles, *Chem. Mater.* 15 (2003) 3873–3878. doi:10.1021/cm034485c.
- [55] M.P.M. Schlesinger, M. Paunovic, M.P. M.Schlesinger, *Modern Electroplating*, John Wiley & Sons, 2011.
- [56] P.P. Lau, C.C. Wong, L. Chan, Improving electroless Cu via filling with optimized Pd activation, *Appl. Surf. Sci.* 253 (2006) 2357–2361. doi:<https://doi.org/10.1016/j.apsusc.2006.05.001>.
- [57] B. Niethammer, Effective Theories for Ostwald Ripening, in: *Anal. Stochastics Growth Process. Interface Model.*, Oxford University Press, 2008. doi:10.1093/acprof:oso/9780199239252.003.0010.
- [58] X.-Y. Guo, B. Zhong, P. Brault, Growth and ripening of two-dimensional palladium islands on Ni (111) surface, *Surf. Sci.* 409 (1998) 452–457. doi:[https://doi.org/10.1016/S0039-6028\(98\)00243-X](https://doi.org/10.1016/S0039-6028(98)00243-X).
- [59] G. Kokkinidis, A. Papoutsis, D. Stoychev, A. Milchev, Electroless deposition of Pt on Ti—catalytic activity for the hydrogen evolution reaction, *J. Electroanal. Chem.* 486 (2000) 48–55. doi:[https://doi.org/10.1016/S0022-0728\(00\)00128-5](https://doi.org/10.1016/S0022-0728(00)00128-5).
- [60] S.M. Ansari, R.D. Bhor, K.R. Pai, D. Sen, S. Mazumder, K. Ghosh, Y.D. Kolekar, C. V

- Ramana, Cobalt nanoparticles for biomedical applications: Facile synthesis, physiochemical characterization, cytotoxicity behavior and biocompatibility, *Appl. Surf. Sci.* 414 (2017) 171–187. doi:<https://doi.org/10.1016/j.apsusc.2017.03.002>.
- [61] M.M. Rahman, S.B. Khan, A. Jamal, M. Faisal, A.M. Aisiri, Iron Oxide Nanoparticles, in: *Nanomaterials*, InTech, 2011. doi:10.5772/27698.
- [62] M. Mallya, R. Shenoy, G. Kodyalamoole, M. Biswas, J. Karumathil, S. Kamath, Absorption spectroscopy for the estimation of glycated hemoglobin (HbA1c) for the diagnosis and management of diabetes mellitus: a pilot study, *Photomed Laser Surg.* 31 (2013) 219–224. doi:10.1089/pho.2012.3421.
- [63] Copper: 04-0836, International Centre for Diffraction Data (JCPDS) , (2010).
- [64] J. Li, X. Yu, T. Shi, C. Cheng, J. Fan, S. Cheng, T. Li, G. Liao, Z. Tang, Depressing of CuCu bonding temperature by composting Cu nanoparticle paste with Ag nanoparticles, *J. Alloys Compd.* 709 (2017) 700–707. doi:10.1016/j.jallcom.2017.03.220.
- [65] G.N. Glavee, K.J. Klabunde, C.M. Sorensen, G.C. Hadjapanayis, Borohydride reductions of metal ions. A new understanding of the chemistry leading to nanoscale particles of metals, borides, and metal borates, *Langmuir.* 8 (1992) 771–773. doi:10.1021/la00039a008.
- [66] D.F. Foust, W. V Dumas, Method for treating polyetherimide substrates and articles obtained therefrom, 1991. US4999251.
- [67] A. Gerbreders, A. Bulanovs, E. Sledevskis, V. Gerbreders, J. Teteris, Photosensitive properties of composite films based on copper chloride in polymer matrix, *IOP Conf. Ser. Mater. Sci. Eng.* 49 (2013) 12032. <http://stacks.iop.org/1757-899X/49/i=1/a=012032>.
- [68] E. Nadal, N. Barros, H. Glenat, J. Laverdant, D.S. Schmool, H. Kachkachi, Plasmon-enhanced diffraction in nanoparticle gratings fabricated by in situ photo-reduction of gold chloride doped polymer thin films by laser interference patterning, *J. Mater. Chem. C.* 5 (2017) 3553–3560. doi:10.1039/C7TC00061H.
- [69] J. Yudelso, H. Gysling, Photosensitive element containing a photoreducible palladium compound and the use thereof in physical development, US3719490A, 1973.
- [70] R. Abargues, K. Abderrafi, E. Pedrueza, R. Gradess, J. Marques-Hueso, J.L. Valdes, J. Martinez-Pastor, Optical properties of different polymer thin films containing in situ synthesized Ag and Au nanoparticles, *New J. Chem.* 33 (2009) 1720–1725. doi:10.1039/B900185A.
- [71] D. Thi My Dung, L. Thi Tuyet Thu, F.-B. Eric, D. Mau Chien, Synthesis and optical

- properties of copper nanoparticles prepared by a chemical reduction method, *Adv. Nat. Sci. Nanosci. Nanotechnol.* 2 (2011) 15009. doi:<https://doi.org/10.1088/2043-6262/2/1/015009>.
- [72] M.D. Susman, Y. Feldman, A. Vaskevich, I. Rubinstein, Chemical Deposition and Stabilization of Plasmonic Copper Nanoparticle Films on Transparent Substrates, *Chem. Mater.* 24 (2012) 2501–2508. doi:10.1021/cm300699f.
- [73] M. El-Kemary, N. Nagy, I. El-Mehasseb, Nickel oxide nanoparticles: Synthesis and spectral studies of interactions with glucose, *Mater. Sci. Semicond. Process.* 16 (2013) 1747–1752. doi:<https://doi.org/10.1016/j.mssp.2013.05.018>.
- [74] E.A. Larios-Rodríguez, F.F. Castellón-Barraza, D.J. Borbón-González, R. Herrera-Urbina, A. Posada-Amarillas, Green-Chemical Synthesis of Monodisperse Au, Pd and Bimetallic (Core-Shell) Au-Pd, Pd-Au Nanoparticles, *Adv. Sci. Eng. Med.* 5 (2013) 665–672. doi:10.1166/ asem.2013.1354.
- [75] M. Radoeva, B. Radoev, Ohm resistivity of electroless copper layers as a function of their thicknesses, *J. Mater. Sci.* 30 (1995) 2215–2219. doi:10.1007/bf01184563.
- [76] J.R. Henry, Electroless (autocatalytic) plating, *Met. Finish.* 98 (2000) 424–435. doi:[http://dx.doi.org/10.1016/S0026-0576\(00\)80351-7](http://dx.doi.org/10.1016/S0026-0576(00)80351-7).
- [77] L.L. Liu, S.M. Ku, C.Y. Chan, K.W. Yee, A potential silver catalyst system for new generation of electroless Cu process as a palladium substitution, 2016 11th Int. Microsystems, Packag. Assem. Circuits Technol. Conf. (2016) 77–80. doi:10.1109/IMPACT.2016.7799980.
- [78] D.F. Foust, W. V Dumas, Polyetherimide Surfaces Chemically Treated To Improve Adhesion to Electroless Copper, in: *Met. Polym.*, American Chemical Society, 1990: pp. 35–485. doi:10.1021/bk-1990-0440.ch035.
- [79] A.J. Frank, N. Cathcart, K.E. Maly, V. Kitaev, Synthesis of Silver Nanoprisms with Variable Size and Investigation of Their Optical Properties: A First-Year Undergraduate Experiment Exploring Plasmonic Nanoparticles, *J. Chem. Educ.* 87 (2010) 1098–1101. doi:10.1021/ed100166g.
- [80] H. Kisch, On the Problem of Comparing Rates or Apparent Quantum Yields in Heterogeneous Photocatalysis, *Angew. Chemie Int. Ed.* 49 (2010) 9588–9589. doi:10.1002/anie.201002653.
- [81] D. Curcó, J. Giménez, A. Addardak, S. Cervera-March, S. Esplugas, Effects of radiation absorption and catalyst concentration on the photocatalytic degradation of pollutants, *Catal. Today.* 76 (2002) 177–188. doi:[https://doi.org/10.1016/S0920-5861\(02\)00217-1](https://doi.org/10.1016/S0920-5861(02)00217-1).

- [82] J. Giménez, D. Curcó, M.A. Queral, Photocatalytic treatment of phenol and 2,4-dichlorophenol in a solar plant in the way to scaling-up, *Catal. Today*. 54 (1999) 229–243. doi:[https://doi.org/10.1016/S0920-5861\(99\)00185-6](https://doi.org/10.1016/S0920-5861(99)00185-6).
- [83] P. Prieto, V. Nistor, K. Nouneh, M. Oyama, M. Abd-Lefdil, R. Díaz, XPS study of silver, nickel and bimetallic silver–nickel nanoparticles prepared by seed-mediated growth, *Appl. Surf. Sci.* 258 (2012) 8807–8813. doi:<https://doi.org/10.1016/j.apsusc.2012.05.095>.